Oligomerization Properties of the Viral Oncoproteins Adenovirus E1A and Human Papillomavirus E7 and Their Complexes with the Retinoblastoma Protein†

Adrienne Clements,‡,§ Karen Johnston,‡ Joan M. Mazzarelli,|| Robert P. Ricciardi,§,|| and Ronen Marmorstein*,‡,§,⊥

The Wistar Institute, Department of Biochemistry and Biophysics, University of Pennsylvania Dental School, and The Department of Chemistry, University of Pennsylvania, Philadelphia, Pennsylvania 19104

Received September 7, 2000; Revised Manuscript Received October 24, 2000

ABSTRACT: Human papillomavirus 16 E7 (HPV16 E7) and adenovirus 5 E1A (Ad5 E1A) are encoded by highly divergent viruses yet are functionally similar in their ability to bind the retinoblastoma (pRB) tumor suppressor protein, causing the aberrant displacement of E2F trancription factors. The amino acid residues of HPV16 E7 that are necessary for stability, for inhibition of pRB function, and for cell transformation are also necessary for E7 oligomerization. However, neither the specific oligomerization state of HPV16 E7 nor of Ad5 E1A as a function of pRB-binding has been characterized. To gain insight into HPV16 E7 and Ad5 E1A oligomerization properties, sedimentation equilibrium experiments were performed with recombinant HPV16 E7 and Ad5 E1A proteins. These studies reveal that, despite the overall functional similarities between these proteins, monomers, dimers, and tetramers of HPV16 E7 were detected while only reversible monomer−dimer association was identified for Ad5 E1A. The apparent $K_{d(monomer-dimer)}$ of HPV16 E7 is approximately 100-fold lower than that of a comparable region of Ad5 E1A, and it is concluded that under physiological protein concentrations HPV16 E7 exists primarily as a dimer. Sedimentation equilibrium experiments of pRB/Ad5 E1A and of pRB/HPV16 E7 complexes demonstrate that the tight association of pRB with the viral oncoproteins does not disturb their inherent oligomerization properties. Taken together, this study demonstrates significant differences between the Ad5 E1A and HPV16 E7 oligomerization states that are potentially related to their distinct structures and specific mechanisms of pRB-inactivation.

The retinoblastoma tumor suppressor protein (pRB) regulates the G1 to S cell cycle transition through its direct association with E2F transcription factors (reviewed in refs *1* and *2*). The unphosphorylated form of pRB represses transcription by binding to E2F (*3*−*6*) and by recruiting histone deacetylases to the promoter regions of S phase-specific genes (*7*−*9*). The phosphorylation of pRB by G1-specific cyclin-CDK complexes leads to the dissociation of E2F and histone deactylases and to the promotion of transcriptional activation of S phase-specific genes (reviewed in refs *1* and *8*). The 928 amino acid pRB protein contains a small pocket region (residues 379−792), comprised of structural domains A and B, which are separated by a flexible and proteolytically sensitive linker region (*10)*. Domains A and B directly interact and, together with an additional C-terminal region, are sufficient for high affinity E2F interaction and transcriptional repression activity (*11*−*15*).

The pRB small pocket region is a hot-spot for mutation in human cancers (reviewed in ref *16*) and is the target of several known DNA viral oncoproteins, including human papillomavirus (HPV) E7 and Adenovirus (Ad) E1A (*17*−*22* and reviewed in ref *16*). HPV E7 and Ad E1A have amino acid sequence homology in three regions that have been designated in Ad E1A as conserved region CR1, CR2, and CR3 (*20*, *23*) and share several properties, including their ability to inactivate pRB (*21*, *24*, *25*). The overall sequence homology between these two proteins is limited, particularly in the CR1 and CR3 regions of E1A compared with the N- and C-terminal regions of E7. However, in this study, these regions of limited homology will be referred to as CR1, CR2, and CR3 in both E1A and E7 to simplify the discussion (Figure 1, panels A and B).

The CR2 region of both proteins contains the LXCXE amino acid sequence (where X is any amino acid, Figure 1, panels A and B) that is necessary for both high affinity pRB interaction (*26*−*32*) and cellular transformation (*26*, *31*). Significantly, HPV E7 is constitutively expressed in cervical carcinomas (*33*, *34*) and HPV E7-pRB interaction is necessary for HPV-mediated cellular transformation (*35*−*40*). As a result of this, E7-derived peptides are currently being investigated as potential components of therapeutic vaccines for cervical cancer (*41*−*45*).

The crystal structure of pRB with a nine amino acid E7-derived peptide revealed that this minimal LXCXE region binds to pRB with a 1:1 stoichiometry and specifically interacts with domain B of the small pocket at a site that is not involved with E2F-binding (*46*). Although the CR2

† This work was supported by an American Cancer Society grant (RPG-98-235-GMC) to R.M., a National Cancer Institute grant (CA29797) to R.P.R and a U.S. Army Breast Cancer Research predoctoral fellowship to A.C. (DAMD17-97-1-7063).

* To whom correspondence should be addressed. Phone: (215) 898-5006. Fax: (215) 898-0381. E-mail: marmor@wistar.upenn.edu.

‡ The Wistar Institute.

§ Department of Biochemistry and Biophysics.

|| University of Pennsylvania Dental School.

⊥ The Department of Chemistry.

10.1021/bi002111g CCC: $19.00
Published on Web 11/23/2000

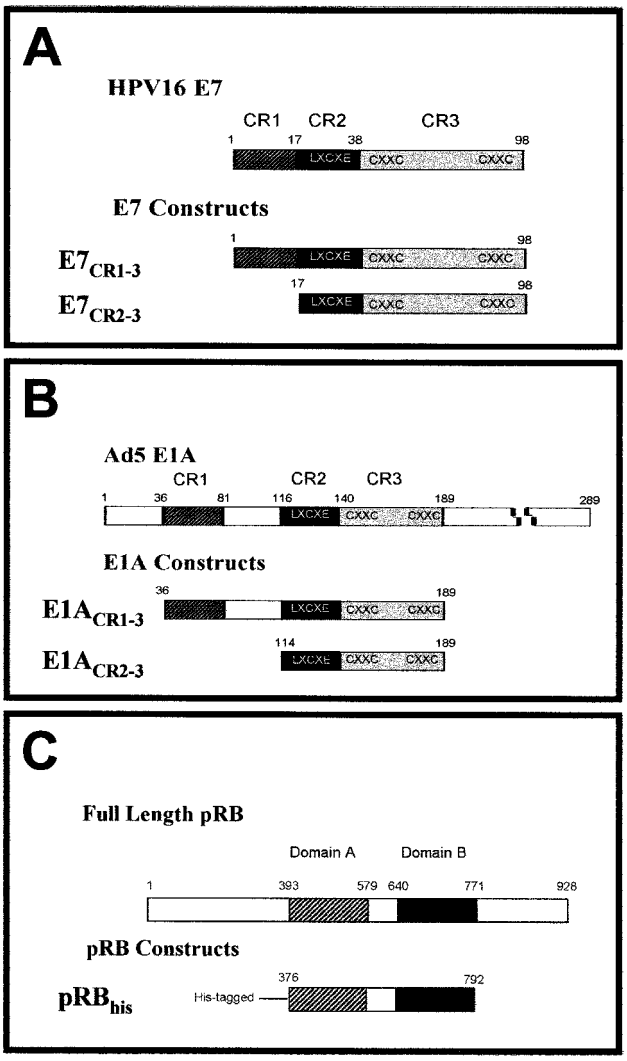

FIGURE 1: Schematic representation of the pRB, HPV16 E7, and Ad5 E1A constructs. One construct of pRB and two constructs of HPV16 E7 and of Ad5 E1A were used in this study. $E7_{CR1-3}$ represents full length HPV16 E7 (amino acids 1−98). $E7_{CR2-3}$ contains the identified pRB-binding domains of HPV16 E7 (amino acids 17−98). $E1A_{CR1-3}$ contains the known pRB-binding domains of Ad5 E1A and contains amino acids 36−189. $E1A_{CR2-3}$ contains amino acids 114−189 of Ad5 E1A. pRB_{his} contains an amino terminal 6x histidine tag and includes the minimal viral oncoprotein binding region of pRB (domain A through domain B, residues 376−792). It is important to note that there is limited homology between the three domains of the viral proteins. The viral proteins are labeled identically in this study to simplify the discussion.

region is necessary for pRB interaction, short peptides of viral oncoproteins containing only this region are not capable of displacing E2F transcription factors from pRB (*22*, *47*), suggesting that these viral oncoproteins have additional pRB-binding sites. In support of this, the apparent dissociation constant (K_d) for an HPV16 E7 CR2-derived peptide complexed with GST-pRB60[1] is approximately 200 nM whereas the apparent K_d for the full-length HPV16 E7/pRB60 complex is significantly lower at 1.3 nM (*29*, *46*).

The CR3 regions of HPV E7 and Ad E1A also share similarity. While there is low overall sequence homology in this region, the domains from both proteins contain two CXXC sequences that bind zinc (*48*−*53*, Figure 1, panels A and B). In addition, the CR3 region of both HPV E7 and Ad E1A contain transactivation function and interact with TATA box-binding protein (TBP) (*54*−*58*) and, in the case of E1A, the mediator complex (*59*).

Despite their similar capacity to inhibit pRB function, HPV E7 and Ad E1A have different mechanisms for achieving this effect. First, the specific mechanisms of E2F displacement are distinct for each of the two proteins. Studies with Ad E1A-derived peptides demonstrate that the first half of CR1 interacts with pRB at a site that is different from the CR2 region, which is necessary for E2F displacement and transcriptional activation (*30*, *32*, *60*). In contrast, with HPV E7, it is the CR3 region that binds to pRB and is required for E2F displacement (*61*−*63*). Second, HPV E7 expression is directly linked to pRB degradation (*64*−*66*), while the expression of Ad E1A is not (*65*).

Studies of bacterially expressed HPV16 E7 demonstrate that it exists as an oligomer in solution (*51*, *67*), and deletion and mutational analysis demonstrate that this oligomerization is mediated by the CR3 region of HPV E7 (*27*, *68*). Significantly, mutations that prevent HPV E7 oligomerization also lead to E7 instability and disrupt the cell transforming properties of E7 (*27*, *37*, *39*, *40*). Despite the apparent importance of E7 oligomerization for efficient and complete pRB-binding and cell transformation, the specific oligomerization state of HPV E7 or Ad E1A, in the absence or presence of pRB has not been investigated.

To gain insight into the oligomerization state of HPV E7 and Ad E1A, we have prepared and purified to homogeneity recombinant HPV16 E7 and Ad5 E1A proteins and have employed sedimentation equilibrium experiments. We also have extended these studies to recombinantly prepared pRB/HPV16 E7 and pRB/Ad5 E1A complexes. Our studies reveal that, at physiological protein concentrations, the HPV16 E7 recombinant protein exists predominately as a dimer while a comparable region of Ad5 E1A exists primarily as a monomer. In addition, a comparison of the sedimentation equilibrium results with gel filtration elution profiles suggests that both proteins adopt an elongated shape in solution. We also show that pRB interacts with Ad5 E1A as a 1:1 complex, while it interacts with HPV16 E7 as a larger complex that is most consistent with the presence of two or four molecules of HPV16 E7 bound to two molecules of pRB. The different oligomerization properties of the related HPV E7 and Ad E1A proteins may contribute to their distinct modes of pRB inhibition.

MATERIALS AND METHODS

Cloning of HPV16 E7, Ad5 E1A, and pRB Constructs. The following constructs used in this study are summarized in Figure 1. Cloning of $E7_{CR1-3}$ (HPV16 E7, amino acids 1−98), $E1A_{CR1-3}$ (Ad5 E1A, amino acids 36−189), $E1A_{CR2-3}$ (Ad5 E1A, amino acids 114−189), and pRB_{his} (a 6× histidine-tagged amino terminal pRB construct with amino acids 376−792) into pET or pRSET expression vectors and subcloning of pRB_{his} into the coexpression vector pRM1 was performed as previously described (*69*). $E7_{CR2-3}$ (HPV16 E7, amino acids 17−98) was cloned essentially as described for $E1A_{CR1-3}$ with the following exceptions.

[1] Abbreviations: GST-pRB60, a glutathione *S*-transferase fusion protein with a pRB region containing domain A through the C-terminus; SDS−PAGE, sodium dodecyl sulfate−polyacrylamide gel electrophoresis; IPTG, isopropyl-β-D-thiogalactopyranoside.

Primers E7_17_5 (5′-GGGAATTCCATATGAATCCA-GAGACAACTGATCTCTAC-3′) and E7_98_3 (5′-CGCG-GATCCTTATGGTTTCTGAGAACAGATGGG3′) were used to amplify the gene encoding $E7_{CR2-3}$ from pET-$E7_{CR2-3}$ and to introduce 5′ *Nde*I and 3′*Bam*HI restriction sites (underlined). Primer E7_17_5 also encoded a methionine and an asparagine directly N-terminal to amino acid 17 for optimal expression. All constructs were verified by sequencing at the University of Pennsylvania DNA sequencing facility.

Expression and Purification of $E7_{CR1-3}$, $E7_{CR2-3}$, and $E1A_{CR2-3}$. BL21(DE3) cells were transformed with pET-$E7_{CR1-3}$ vector for protein overexpression. The vector-transformed cells were grown in LB media with 100 μg/mL ampicillin at 37 °C. When the A_{595nm} of the cultures reached 0.5−0.7, 1 mM IPTG was added to the cells for protein induction. Since E7 and E1A are both zinc-binding proteins, 100 μM zinc acetate was added to the cultures during protein induction. After incubation at 37 °C for three additional hours, the cells were harvested by centrifugation at 4000*g* for 20 min. Purification steps for $E7_{CR1-3}$ and all other proteins were performed at 4 °C. The $E7_{CR1-3}$ cell pellet was resuspended in buffer A (20 mM Hepes, pH 7.9, 150 mM sodium chloride, 10 μM zinc acetate, and 10 mM dithiothreitol) and lysed by sonication. The $E7_{CR1-3}$ lysate was centrifuged for 20 min at 40000*g*. Coomassie blue stained SDS−PAGE revealed that recombinant $E7_{CR1-3}$ existed in the soluble fractions. The cleared lysate containing $E7_{CR1-3}$ was loaded onto a Q-sepharose anion-exchange column that was preequilibrated with buffer A. After washing with 10−20 column volumes of buffer A, $E7_{CR1-3}$ was eluted from the column with a 150−700 mM sodium chloride gradient. Fractions containing $E7_{CR1-3}$ were pooled and ammonium sulfate was added to the pooled fractions until it reached a final concentration of 0.7 M. The protein sample was loaded onto a phenyl sepharose column equilibrated with buffer A plus 0.7 M ammonium sulfate. $E7_{CR1-3}$ was eluted from the phenyl sepharose column with a 0.7 to 0 M ammonium sulfate gradient. The fractions containing $E7_{CR1-3}$ were pooled and concentrated using a centrifugal filter. The sample of $E7_{CR1-3}$ was further purified by size-exclusion chromatography using a high load Superdex 200 prep-grade column (Amersham Pharmacia Biotech) in buffer B (20 mM Tris, 8.5, 100 mM sodium chloride and 20 mM dithiothreitol).

The purification protocol for recombinant $E7_{CR2-3}$ was essentially as described for $E7_{CR1-3}$ except that the protein was eluted from the ion-exchange column with a 150−850 mM sodium chloride gradient. The purification protocol for recombinant $E1A_{CR2-3}$ was essentially as described for $E7_{CR1-3}$ except that buffer A plus 1 M ammonium sulfate was used during the phenyl sepharose purification step and the gel filtration purification step was performed with a high load Superdex 75 prep-grade column (Amersham Pharmacia Biotech). All proteins were concentrated to 15−30 mg/mL using a centrifugal filter and stored at −70 °C until further use.

Expression and Purification of pRB_{his}. BL21(DE3) cells were transformed with pRSET-pRB_{his} for protein expression. Cell cultures were grown in LB media plus 100 μg/mL ampicillin at 37 °C until the A_{595nm} reached 0.15−0.2. The temperature was then lowered to 15 °C. When the A_{595nm} reached 0.5−0.7, 100 μM magnesium chloride and 1 mM IPTG were added to the culture for protein induction. After 12 additional hours, the cells were harvested and pelleted by centrifugation at 4000*g* for 20 min. The cell pellet was resuspended in buffer C (20 mM Hepes, pH 7.2, 200 mM sodium chloride, 10 μM magnesium chloride, and 10 mM β-mercaptoethanol) and lysed by sonication. The lysate was centrifuged at 40000*g* for 20 min. Coomassie blue stained SDS−PAGE analysis revealed that recombinant pRB_{his} existed primarily in the soluble fractions. The pRB_{his} protein was then loaded onto a nickel agarose column equilibrated with buffer C. After washing with 20 column volumes of buffer C, pRB_{his} was eluted from the nickel column with a 0−0.5 M imidazole (pH 7.2) gradient to separate pRB from impurities that bound the column with low affinity. The protein fractions containing pRB_{his} were pooled and concentrated using a centrifugal filter. The protein was further purified by size-exclusion chromatography using a high load Superdex 200 prep-grade gel filtration column in buffer C. The gel filtration peak fractions containing pRB_{his} were pooled and concentrated to 20 mg/mL using a centrifugal concentrator and stored at −70 °C until further use.

Coexpression and Copurification of $pRB_{his}/E1A_{CR1-3}$ and $pRB_{his}/E7_{CR2-3}$ Complexes. BL21(DE3) cells were transformed with the pRM1-pRB_{his} vector, made competent, and subsequently transformed with pRSET-$E1A_{CR1-3}$ for protein coexpression. Cell cultures of the cotransformed cells were grown in LB media in the presence of 200 μg/mL ampicillin and 50 μg/mL kanamycin at 37 °C. When the A_{595nm} reached 0.15−0.2, the growth temperature was reduced to 15 °C. At an A_{595nm} of 0.5−0.7, 100 μM zinc acetate, 100 μM magnesium chloride (*69*) and 1 mM IPTG were added for protein induction. After approximately 12 h, the cells were harvested by centrifugation (4000*g*, 20 min). The cell pellet containing $pRB_{his}/E1A_{CR1-3}$ was resuspended in buffer E (20 mM Hepes, pH 7.5, 200 mM sodium chloride, 10 mM β-mercaptoethanol, 10 μM magnesium chloride, 10 μM zinc acetate, and 25 mM imidazole, pH 7.5) and lysed by sonication. The lysate was centrifuged at 40000*g* at 4 °C. Coomassie blue stained SDS−PAGE analysis revealed that the $pRB_{his}/E1A_{CR1-3}$ complex was in the soluble fraction. The supernatant was then mixed with Ni−NTA agarose resin (equilibrated with buffer E) for an hour with gentle agitation and the slurry was subsequently packed in a column. The column was washed with 20−30 column volumes of buffer E and the proteins were coeluted from the column with a 0.025 to 0.5 M imidazole gradient. The fractions containing the $pRB_{his}/E1A_{CR1-3}$ complex were pooled with the addition of 20 mM dithiothreitol. The complex was concentrated using a centrifugal filter and further copurified by size-exclusion chromatography using a high load Superdex 200 prep-grade gel filtration column in buffer G (20 mM Hepes, pH 7.5, 200 mM sodium chloride, and 20 mM dithiothreitol). Peak fractions were pooled, concentrated to 2−5 mg/mL and stored at 4 °C until further use.

The coexpression and copurification scheme of the recombinant $pRB_{his}/E7_{CR2-3}$ complex was essentially as described for $pRB_{his}/E1A_{CR1-3}$ except that sonication buffer F (20 mM Hepes, pH 7.5, 200 mM sodium chloride, 10 mM β-mercaptoethanol, 10 μM magnesium chloride, 10 μM zinc acetate and 35 mM imidazole, pH 7.5) was used for cell resuspension and for chromatography on the Ni-NTA agarose column.

Sedimentation Equilibrium Experiment of $E7_{CR1-3}$ and of $E1A_{CR2-3}$ Using Absorption Optics. All sedimentation equilibrium experiments were performed with a Beckman Optima XL-I ultracentrifuge at 4 °C. For $E7_{CR1-3}$, each cell was assembled with a six-channel 12 mm centerpiece and quartz windows. Purified $E7_{CR1-3}$ was dialyzed against a buffer containing 20 mM borate, pH 8.5, and 100 mM sodium chloride for these analytical ultracentrifugation experiments. Borate was used in this experiment because it does not significantly absorb at λ_{230nm}. The cell channels were loaded with either sample or reference dialysis buffer. A total of nine protein samples were loaded. However, since five of the starting concentrations were out of detection range, only four samples of the dialyzed protein were analyzed with starting concentrations of 0.025, 0.075, 0.25 and 0.50 mg/mL. The two speed experiment was performed at 25 800 and at 36 500 rpm. Absorbance scans were performed on the samples every 4 h until the samples reached equilibrium. Scans for the two lower protein concentrations were recorded at λ_{230nm} and scans for the two higher protein concentrations were recorded at $\lambda_{280\ nm}$.

For the $E1A_{CR2-3}$ experiment, each cell was assembled with a double-sector 12 mm centerpiece and with quartz windows. For this experiment, absorbance scans at λ_{280nm} were taken for three samples starting protein concentrations of 0.60, 0.38 and 0.23 mg/mL. This single speed experiment was performed at 48 000 rpm. For these and all other experiments, equilibrium was assessed by comparison of successive scans using the MATCH program and data editing was performed using the REEDIT program for this and all subsequent analytical ultracentrifugation experiments (both programs were provided by National Analytical Ultracentrifugation Facility, Storrs, Connecticut).

Sedimentation Equilibrium Experiments of $E7_{CR1-3}$, $E1A_{CR2-3}$, and pRB_{his} Using Interference Optics. For this and all other sedimentation equilibrium experiments using interference optics, each cell was assembled with a double-sector 12 mm centerpiece and with sapphire windows. Blank scans with distilled water were taken before all interference optics sedimentation equilibrium experiments at appropriate speeds to correct for window distortion of the fringe displacement data (*72*). Cells were loaded with either $E7_{CR1-3}$ or $E1A_{CR2-3}$ and reference buffer B. Purified samples of $E7_{CR1-3}$ were loaded at concentrations of 1 mg/mL and 0.5 mg/mL for a two speed study at 25 800 and 36 500 rpm. The $E1A_{CR2-3}$ experiment was performed at 40 000 rpm with starting protein concentrations of 0.77, 0.5, and 0.20 mg/mL. For pRB_{his}, cells were loaded at three different protein concentrations with reference buffer C for two separate sedimentation equilibrium experiments at 18 000 and at 25 000 rpm. The loading concentrations of pRB_{his} were 2, 1, and 0.5 mg/mL for the experiment at 18 000 rpm. The pRB_{his} loading concentrations were 1.2, 0.6, and 0.3 mg/mL for the experiment at 25 000 rpm. Fringe displacement scans were collected every 4 h until the protein samples reached equilibrium.

Sedimentation Equilibrium Experiments of $pRB_{his}/E7_{CR2-3}$ and of $pRB_{his}/E1A_{CR1-3}$ Complexes Using Interference Optics. Cells were loaded with either the $pRB_{his}/E7_{CR2-3}$ complex or the $pRB_{his}/E1A_{CR1-3}$ complex and reference buffer G. Purified samples of the $pRB_{his}/E7_{CR2-3}$ complex were loaded at three different concentrations for two separate experiments. The first experiment was at 18 000 rpm with loading concentrations of 1, 0.5, and 0.25 mg/mL and the second experiment was at 20 000 rpm with loading concentrations of 1, 0.6, and 0.4 mg/mL. Purified samples of the $pRB_{his}/E1A_{CR1-3}$ complex were loaded at three different concentrations for two experiments. One experiment was performed at 18 500 rpm with loading concentrations of 2, 1.5, and 1 mg/mL and the other experiment was performed at 18 700 rpm with loading concentrations of 1.3, 0.7, and 0.5 mg/mL. Fringe displacement scans were collected every 4 h until the protein samples reached equilibrium.

Data Analysis of Sedimentation Equilibrium Experiments. After equilibrium was obtained, the NONLIN program (*70*) was used to globally fit several scans for each set of experiments. NONLIN fits using an effective reduced molecular weight, $\sigma = M(1 - \bar{\nu}\rho)\omega^2/RT$, in which M is the molecular weight, $\bar{\nu}$ is the partial specific volume of the protein, ρ is the solvent density, ω is the angular velocity $[2\pi(\text{rpm})/60]$, R is the gas constant, and T is the temperature in kelvin. The partial specific volume of all the proteins in this study was calculated from the amino acid sequence while the density of the solvent was calculated as described (*71*). For each set of experiments, an initial single species model was used to estimate the effective reduced molecular mass of the proteins. Although the overall fit quality for the single species model was poor for all of the experiments, it was sufficient to provide an apparent weight-average molecular mass ($M_{w,app}$) for the proteins in the sample. For models of associating systems, σ was held at the correct value based on the known monomer molecular weight of the proteins and equilibrium constants were fitted as ln K. These values then were converted to dissociation constants with the appropriate molar units. The fit quality of the models for all of the experiments was determined by examination of residuals and by minimization of the fit variance. Fits were not improved by including B factors in the models. Therefore, it is assumed that protein nonideality was not a factor at the concentrations tested. Results are summarized in Table 1.

RESULTS

Purification of $E7_{CR1-3}$ and of $E7_{CR2-3}$ and Sedimentation Equilibrium Experiments of Recombinant $E7_{CR1-3}$. Full-length HPV16 E7 (Figure 1A, $E7_{CR1-3}$) was expressed as soluble protein in bacteria at 37 °C. $E7_{CR1-3}$ was purified using a combination of Q sepharose anion-exchange chromatography, separation based on hydrophobicity using a phenyl-sepharose column and size-exclusion chromatography using a high load Superdex 200 prep-grade gel filtration column. Peak protein fractions that eluted from the gel filtration column contained $E7_{CR1-3}$ and appeared to be greater than 95% pure (Figure 2A). Although the monomer molecular mass of $E7_{CR1-3}$ is 11.0 kDa, purified $E7_{CR1-3}$ eluted from the gel filtration column in one peak between the elution points of protein standards with molecular masses of 158 and 44 kDa (Figure 2A). The large hydrodynamic radius of $E7_{CR1-3}$ suggested that it may be an oligomer containing two or more subunits and/or has an elongated asymmetric shape. The purification scheme of $E7_{CR2-3}$ [monomer molecular mass (M) = 9.29 kDa] was essentially the same as $E7_{CR1-3}$. The gel filtration elution point of $E7_{CR2-3}$ demonstrated that the hydrodynamic radius of $E7_{CR2-3}$ is only slightly smaller than that of $E7_{CR1-3}$ (Figure 2A), suggesting that it has similar oligomeric properties and/or shape as $E7_{CR1-3}$. It is important to note that these protein

Table 1: Apparent Dissociation Constants (K_d) of $E7_{CR1-3}$, $E1A_{CR2-3}$, pRB_{his}, the $pRB_{his}/E7_{CR2-3}$ Complex, and the $PRB_{His}/E1A_{CR1-3}$ Complex

protein	n^a	$K_{d(monomer-dimer)}$ (M)	$K_{d(dimer-tetramer)}$ (M)	rms[b] ($\times 10^{-3}$)	monomer M (kDa)	$M_{w,app}$[c] (kDa)
$E7_{CR1-3}$ (A)	8	1.1×10^{-6} [d] (6.7×10^{-7}, 1.8×10^{-6})[e]	3.6×10^{-3} [d] (2.5×10^{-3}, $1.8 \times 10-2$)[e]	5.9	11.0	19.9
$E7_{CR1-3}$ (B)	4	na[f]	5.5×10^{-4} ($\pm$ 2.8)[g] (2.5×10^{-4}, $9.1 \times 10-4$)[h]	9.9	11.0	24.9
$E1A_{CR2-3}$	6	1.4×10^{-4} ($\pm$ 0.52)[g] (5.5×10^{-5}, $1.8 \times 10-4$)[h]	na[i]	3.4	8.77	11.6
pRB_{his}	6	1.3×10^{-3} ($\pm$ 0.52)[g] (5.5×10^{-4}, $2.0 \times 10-3$)[h]	na[i]	9.9	49.9	52.0
pRB_{his}/viral oncoprotein complex	n^a	$K_{d(1:1-2:2)}$ (M)	$K_{d(2:2-4:4)}$ (M)	rms[b] ($\times 10^{-3}$)	M of a 1:1 complex (kDa)	$M_{w,app}$[c] (kDa)
$pRB_{his}/E7_{CR2-3}$	6	8.3×10^{-7} ($\pm$ 5.2)[g] (2.4×10^{-7}, $1.8 \times 10-6$)[h]	3.8×10^{-5} ($\pm$2.5)[g] (1.2×10^{-5}, 7.4×10^{-5})[h]	9.4	59.3	130
$pRB_{his}/E1A_{CR1-3}$	6	1.1×10^{-4} ($\pm$ 0.56)[g] (6.6×10^{-5}, 2.1×10^{-4})[h]	n.a.[j]	8.9	67.1	80.2

[a] Number of samples from discrete concentrations and/or different centrifugation speeds analyzed simultaneously. [b] Root-mean-square deviation of the residuals for the multiple species models. [c] The apparent weight-average molecular mass determined by using a single species model for *n* samples. It is important to note that the overall quality of fit for every single species model was lower than the fit quality of the multiple species models. [d] A global K_d estimated for *n* samples analyzed simultaneously. [e] Corresponds to a 95% confidence interval or $\pm$ 2 SD from the global K_d. [f] Not applicable due to the absence of monomer in the best model for the speed and concentration range of this experiment. [g] The average K_d ($\pm$ SD) of a model in which *n* samples were analyzed simultaneously while fitting individual dissociation constants. [h] Corresponds to the minimum and maximum values of individual dissociation constants for n samples. [i] Not applicable due to the absence of tetramer in the best model for the speed and concentration range of this experiment. [j] Not applicable due to the absence of a 4:4 complex in the best model for the speed and concentration range of this experiment.

preparations were performed multiple times with highly reproducible results.

To investigate the oligomerization state of $E7_{CR1-3}$, two sets of sedimentation equilibrium experiments were performed with the purified protein. The first set of experiments was performed at 28 500 and 36 500 rpm at 4 °C using absorbance optics. The same protein samples with four different starting concentrations ranging from 0.025 to 0.50 mg/mL were used for both speeds. This provided eight samples from discrete concentrations and/or different centrifugation speeds for simultaneous analysis using nonlinear regression (*70*). After all of the protein samples reached equilibrium, the eight data plots representing the protein concentration versus radius were initially fitted with a single species model to determine the apparent weight-average molecular weight ($M_{w,app}$) of the system. Although this gave a poor fit to the data, the $M_{w,app}$ for $E7_{CR1-3}$ was 19.9 kDa (Table 1), suggesting that $E7_{CR1-3}$ self-associates (M =11.0 kDa). Data analysis resulted in two models describing self-association that fit equally well. One model included monomers, dimers and tetramers while the second model described monomers, dimers and trimers. Both fits were significantly better than models describing only monomers and dimers. For this experiment, all eight samples were analyzed simultaneously, while fitting global apparent dissociation constants, to develop a model for reversible monomer−dimer−trimer or monomer−dimer−tetramer (Figure 2B) equilibrium. For the monomer−dimer−tetramer model, the apparent dissociation constants, $K_{d(monomer-dimer)}$ and $K_{d(dimer-tetramer)}$, were 1.1 μM and 3.6 mM, respectively (Table 1).

To distinguish between the monomer−dimer−trimer and the monomer−dimer−tetramer model for $E7_{CR1-3}$, a second set of experiments at higher protein concentrations was performed. This set of experiments with $E7_{CR1-3}$ was performed using interference optics with two different starting protein concentrations of 0.5 mg/mL and 1.0 mg/mL. This two speed study was performed at 25 800 and 36 500 rpm. When all of the protein samples reached equilibrium, four data plots (from the two different protein concentrations and the two speeds) were initially fitted with a single species model to determine the $M_{w,app}$ of 24.9 kDa for the system (Table 1). The best model for this set of experiments described only dimers and tetramers in solution. All four samples were globally analyzed, using nonlinear regression (*70*), while fitting individual apparent dissociation constants, to develop a model for dimer−tetramer equilibrium (Figure 2C). Unlike the first set of experiments, this model was significantly better than a monomer-trimer model or any other models containing three species. Monomeric protein could not be included in this model, presumably because of the higher protein concentration. The apparent dissociation constant, $K_{d(dimer-tetramer)}$, for the protein was 550 μM $\pm$ a standard deviation (SD) of 280 μM (Table 1).

Although both sets of experiments suggest that $E7_{CR1-3}$ is predominantly a dimer, the $K_{d(dimer-tetramer)}$ differ significantly between the two experiments. Therefore, it is not clear whether dimer−tetramer association is reversible. The first set of experiments was performed at an optimal protein concentration for monomer detection, while the second set was designed to probe dimer−tetramer association. It is possible that the amount of higher oligomer in the first experiment was too low to obtain an accurate $K_{d(dimer-tetramer)}$ estimate. Therefore, based on both sets of experiments, it can be concluded that the $K_{d(dimer-tetramer)}$ of $E7_{CR1-3}$ is at least 550 $\pm$ 280 μM. These values are weak enough to suggest that the dimer−tetramer equilibrium does not occur at physiological protein concentrations.

Purification and Sedimentation Equilibrium Experiments of Recombinant $E1A_{CR2-3}$. To directly compare the oligomerization properties of Ad5 E1A and HPV16 E7, we initially sought to purify and characterize $E1A_{CR1-3}$, which

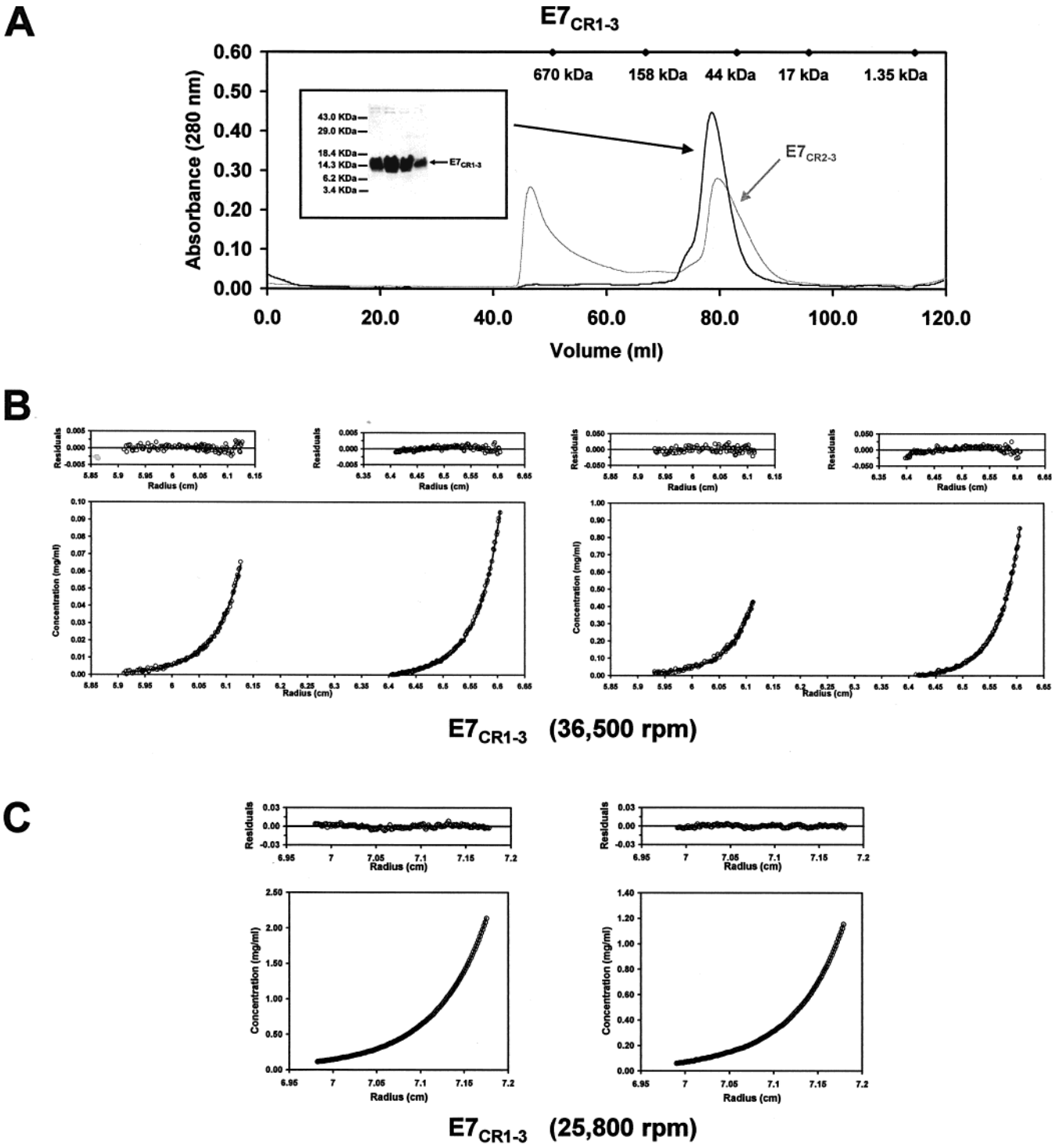

FIGURE 2: Purified recombinant $E7_{CR1-3}$ exists primarily as a dimer. (A) Final purification step of recombinant $E7_{CR1-3}$ and $E7_{CR2-3}$ using size-exclusion chromatography. An 18% Coomassie-blue stained SDS−PAGE analysis of four peak fractions reveal that purified recombinant $E7_{CR1-3}$ elutes from a high load Superdex 200 prep-grade size-exclusion column between the elution points of protein standards with molecular masses of 158 and 44 kDa. The $E7_{CR1-3}$ monomer molecular mass is calculated to be 11.0 kDa based on the protein sequence. For comparison, the $E7_{CR2-3}$ elution point is shown in gray [the peak height is scaled down to facilitate peak comparison; monomer molecular mass (M) = 9.29 kDa]. The first large peak in the $E7_{CR2-3}$ elution profile contains high molecular weight contaminants. (◆) The peak elution points of protein standards. (B) Sedimentation equilibrium analysis of $E7_{CR1-3}$ at low protein concentrations. This set of sedimentation equilibrium experiments was performed at 25 800 and at 36 500 rpm and 4 °C. Absorbance scans from eight samples with different loading concentrations and/or centrifugation speeds were analyzed simultaneously with a model describing monomeric, dimeric and tetrameric species using the nonlinear regression program NONLIN (*70*). The fits for the four samples at 36 500 rpm are shown. The bottom panels illustrate the calculated fits for the samples as continuous lines. (○) Data points are represented. The top panels represent residuals for the calculated fit. (C) Sedimentation equilibrium analysis of $E7_{CR1-3}$ at high protein concentrations. This 4 °C two speed sedimentation equilibrium experiment was performed at 25 800 and at 36 500 rpm. Fringe displacement data for two different concentrations at both speeds were analyzed simultaneously with a model describing dimeric and tetrameric species using NONLIN (*70*). The fits for the two samples at 25 800 rpm are shown. The bottom panel illustrates the calculated fits as continuous lines. (○) Data points are represented. The top two panels represent the residuals for the calculated fits.

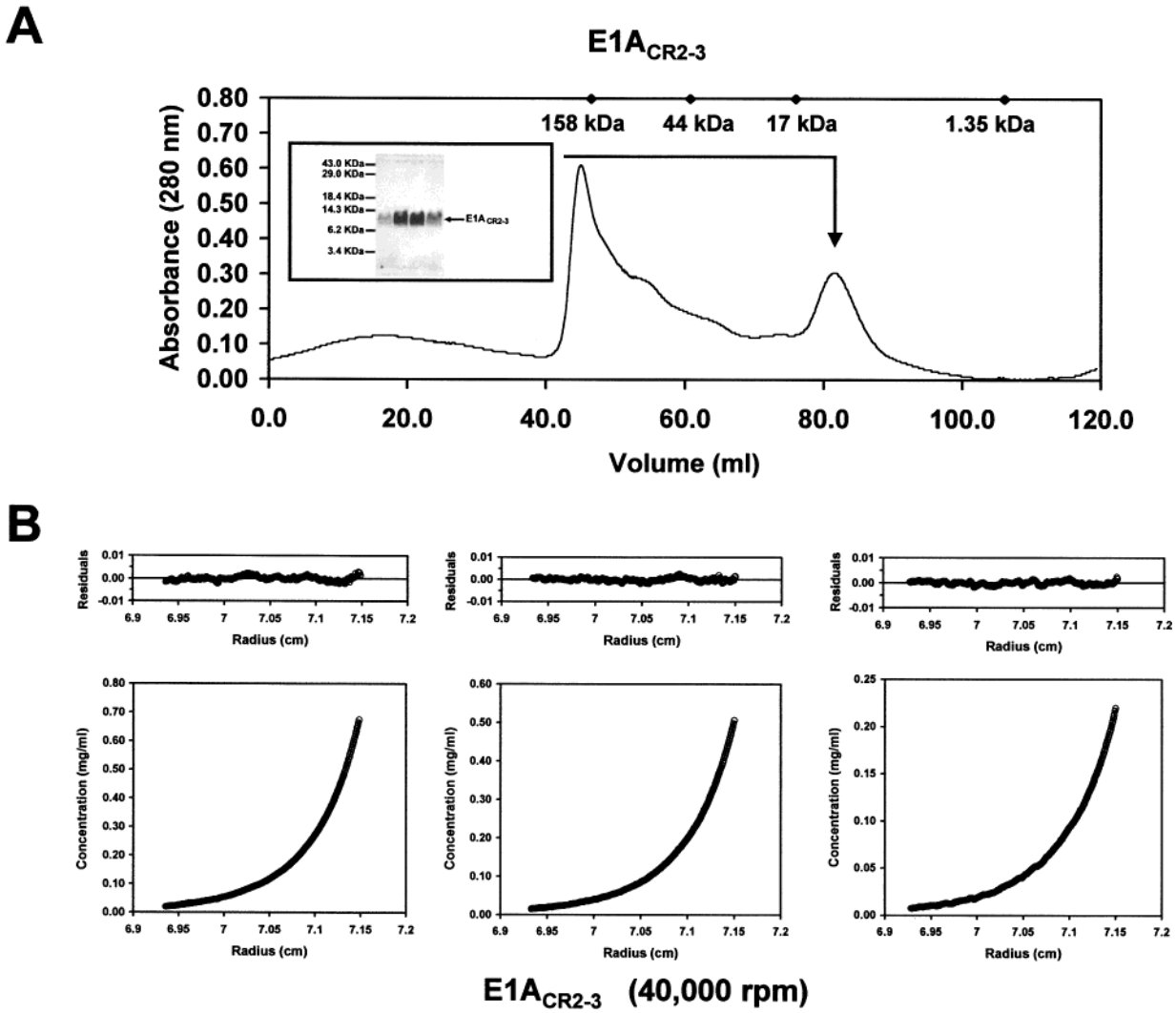

FIGURE 3: Purified recombinant E1A$_{CR2-3}$ exists primarily as a monomer. (A) Final purification step of recombinant E1A$_{CR2-3}$ using size-exclusion chromatography. An 18% Coomassie-blue stained SDS−PAGE analysis of four peak fractions reveal that purified recombinant E1A$_{CR2-3}$ elutes from a high load Superdex 75 prep-grade size-exclusion column between the elution points of protein standards with molecular masses of 17 and 1.35 kDa. The larger protein peaks represent high molecular weight contaminants separated from the protein of interest. The E1A$_{CR2-3}$ monomer molecular mass is calculated to be 8.77 kDa based on the protein sequence. (◆) The peak elution points of protein standards are represented. (B) Sedimentation equilibrium analysis of E1A$_{CR2-3}$ with two speeds and multiple protein concentrations. Two single speed sedimentation equilibrium experiments with separately prepared protein were performed at 40 000 and at 48 000 rpm and 4 °C. Three samples collected with fringe displacement data and three samples obtained from A_{280nm} scans from different loading concentrations were analyzed simultaneously with a model describing monomeric and dimeric species using NONLIN (*70*). The samples from the experiment at 40 000 rpm are shown. The bottom panel illustrates the calculated fits as continuous lines. (○) Data points for the scans are represented. The top three panels represent residuals for the calculated fits.

contains the CR1 region through the CR3 region (Figure 1B). However, protein purification of E1A$_{CR1-3}$ was problematic and this protein eluted from the Superdex 200 gel filtration column as a broad series of aggregates (data not shown). Therefore, Ad5 E1A$_{CR2-3}$ (Figure 1B) was used for these studies. This construct was expressed in soluble form in bacteria at 37 °C. E1A$_{CR2-3}$ was purified using a combination of Q sepharose anion-exchange chromatography, separation based on hydrophobicity using a phenyl-sepharose column and size-exclusion chromatography using a high load Superdex 75 prep-grade gel filtration column. The gel filtration column typically yielded protein peaks of high molecular weight contaminants followed by a single peak containing E1A$_{CR2-3}$ (Figure 3A). Peak E1A$_{CR2-3}$ fractions that eluted from the gel filtration column appeared to be greater than 95% pure (Figure 3A). This protein preparation was performed multiple times with consistent elution profiles. E1A$_{CR2-3}$, which has a monomer molecular mass of 8.77 kDa, eluted from the gel filtration column in a single peak at a position between protein standards of 17 and 1.35 kDa (Figure 3A) and is consistent with a protein that is larger than 8.77 kDa (approximately 13 kDa) based on the molecular masses of the protein standards. The slightly larger than expected hydrodynamic radius suggests that, like E7$_{CR2-3}$ (Figure 2A), E1A$_{CR2-3}$ has exists as a higher order oligomer and/or has an elongated shape, although it is clear that these properties are distinct from those of E7$_{CR2-3}$.

To probe the oligomerization properties of E1A$_{CR2-3}$, two sedimentation equilibrium experiments were performed with purified E1A$_{CR2-3}$ from separate protein preparations. The first experiment was performed at 40 000 rpm using interference optics with three different starting concentrations, while the second experiment was performed at 48 000 rpm with three different starting concentrations using absorbance

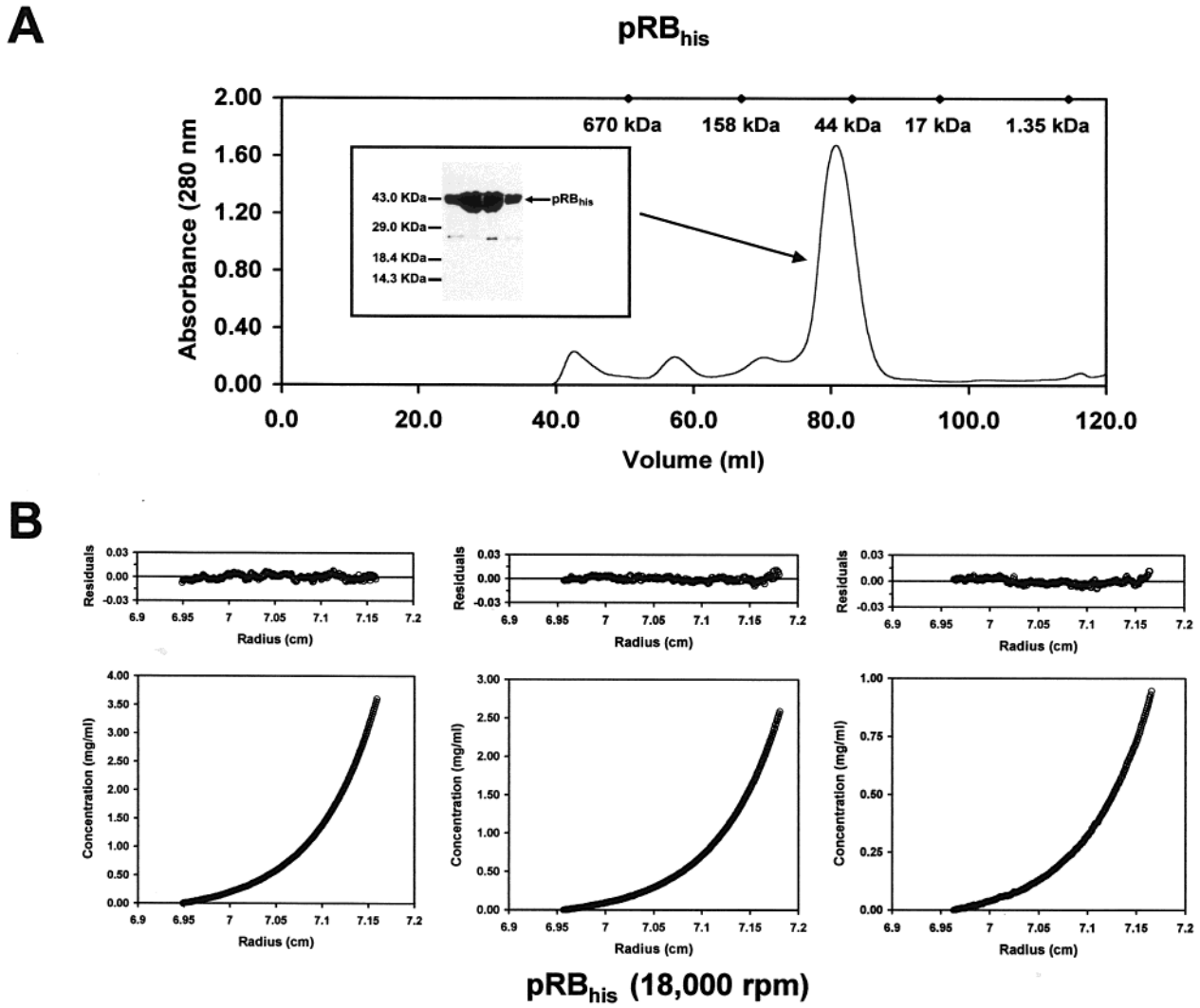

FIGURE 4: Purified recombinant pRB$_{his}$ exists as a monomer. (A) Final purification step of recombinant pRB$_{his}$ using size-exclusion chromatography. A 15% Coomassie-blue stained SDS−PAGE analysis of four peak fractions reveal that purified recombinant pRB$_{his}$ elutes from a high load Superdex 200 prep-grade size-exclusion column at approximately the elution point of the 44 kDa protein standard. The monomer molecular mass of pRB$_{his}$ is calculated to be 49.9 kDa based on the protein sequence. (◆) The peak elution points of protein standards are represented. (B) Sedimentation equilibrium analysis of pRB$_{his}$ from two speeds and with multiple protein concentrations. This set of sedimentation equilibrium experiments were performed at 18 000 and 25 000 rpm at 4 °C. Each experiment was performed with protein from separate preparations. Fringe displacement data of six samples from different loading concentrations and/or different speeds were analyzed simultaneously with a model describing monomeric and a small amount of dimeric species using NONLIN (*70*). The samples from 18 000 rpm are shown. The bottom panel illustrates the calculated fits as continuous lines. (○) Data points for the scans are represented. The top three panels represent residuals for the calculated fits shown.

optics. This provided six samples containing protein from discrete concentrations and/or different centrifugation speeds for data analysis using nonlinear regression (*70*). After all of the protein samples reached equilibrium, the six data plots representing the protein concentration versus radius were simultaneously fitted to the $M_{w,app}$ of 11.9 kDa, suggesting that E1A$_{CR2-3}$ self-association is present (Table 1). Therefore, the six data plots were fitted with models describing self-association. The six samples were analyzed simultaneously to develop a model for monomer−dimer equilibrium (Figure 3B). This fit was significantly better than monomer−trimer models or models containing three oligomeric species. The apparent dissociation constant, $K_{d(monomer-dimer)}$, for the samples was 140 ± 52 μM.

Purification and Sedimentation Equilibrium Experiments of Recombinant pRB$_{his}$. An N-terminal 6× histidine-tagged construct of the pRB small pocket (Figure 1C, pRB$_{his}$) was expressed in soluble form in bacteria at 15 °C. The protein was purified with affinity chromatography (nickel agarose) followed by size-exclusion chromatography using a high load superdex 200 prep-grade gel filtration column. Peak protein fractions that eluted from the gel filtration column contained pRB$_{his}$ and appeared to be greater than 95% pure (Figure 4A). The pRB$_{his}$ protein eluted from the gel filtration column as one peak with a hydrodynamic radius similar to that of the 44 kDa protein standard (Figure 4A). The monomer molecular mass of this pRB region is 49.9 kDa, suggesting that the protein eluted from the gel filtration column as a monomer.

Two sedimentation equilibrium experiments were performed with pRB$_{his}$ at 18 000 and 25 000 rpm using interference optics and three different protein concentrations. When all of the protein samples reached equilibrium, the six separate data plots representing the protein concentration versus radius were fitted with a single species model to determine the $M_{w,app}$ of 52.0 kDa. Although the $M_{w,app}$ was

within the 5% expected experimental error of the actual monomer molecular weight, the residuals from this single-species model were nonrandom and suggested that slight aggregation was present. The data plots were then fitted to a model describing very weak self-association using nonlinear regression (70). The model describing self-association was significantly better than the single species model. Therefore, all six samples were analyzed simultaneously to develop a model for very weak monomer−dimer equilibrium (Figure 4B). The apparent dissociation constant, $K_{d(monomer-dimer)}$, for the samples was 1.4 ± 0.52 mM (Table 1), demonstrating that this pRB domain is primarily monomeric.

Purification and Sedimentation Equilibrium Experiments of the Recombinant $pRB_{his}/E7_{CR2-3}$ Complex. For complex formation, pRB_{his} and $E7_{CR2-3}$ were coexpressed in bacteria as described (*69*). Coexpression was utilized for this study because the stoichiometry of binding between the pRB_{his} and E7 were unknown, and at high protein concentrations, precipitation would occur upon mixing the individually purified proteins (*69*). Initially, we tried to coexpress and copurify pRB_{his} with $E7_{CR1-3}$ for further characterization. Unfortunately, the purified $pRB_{his}/E7_{CR1-3}$ complex yields were too low for analytical ultracentrifugation experiments (data not shown). Therefore, a construct of HPV16 E7 ($E7_{CR2-3}$, Figure 1A), containing the minimal pRB-binding domain (CR2) and the low affinity pRB-binding site (CR3), was coexpressed with pRB_{his} and used for these studies (*69*). pRB_{his} was coexpressed with $E7_{CR2-3}$ and the complex was purified to homogeneity at a sufficient yield for analytical ultracentrifugation experiments. The complex was expressed at 15 °C in bacteria. The proteins existed in the soluble fraction and were copurified through a combination of affinity chromatography (nickel agarose) and size-exclusion chromatography using a high load Superdex 200 prep-grade gel filtration column. The proteins coeluted from the gel filtration column at a molecular mass that was consistent with the 158 kDa protein standard and had a significantly larger hydrodynamic radius than that of individually purified pRB_{his} or of purified $E7_{CR2-3}$ proteins (Figure 5A). The crystal structure of the pRB small pocket with an $E7_{CR2}$ -derived peptide suggests that the stoichiometry of pRB/E7 binding is 1:1 (*46*). Assuming that this $pRB_{his}/E7_{CR2-3}$ complex exists with 1:1 stoichiometry, the predicted molecular mass would be 59.3 kDa. Therefore, the gel filtration elution profile suggests that this complex exists at an oligomerization state that is greater than 1:1 or that the shape of the complex is elongated. This purification protocol was performed multiple times with reproducible results. In addition, the elution point of gel-filtered $pRB_{his}/E7_{CR2-3}$ complex is similar to the $pRB_{his}/E7_{CR1-3}$ complex (data not shown), suggesting that the oligomerization properties and shape of the two complexes are similar.

To evaluate the oligomerization state of the $pRB_{his}/E7_{CR2-3}$ complex, two sedimentation equilibrium experiments from two separate protein preparations were performed at 18 000 and at 20 000 rpm with interference optics. Three different starting concentrations of purified complex were used for each experiment, providing six different samples for data analysis. After all samples reached equilibrium, all six data plots representing the protein concentration versus radius were fitted to a single species model to determine the overall $M_{w,app}$ of 130 kDa for the system using nonlinear regression analysis (*70*). Since the $M_{w,app}$ was significantly higher than that of a 1:1 $E7_{CR2-3}/pRB_{his}$ complex, the six plots were analyzed to develop models for self-association. The data were analyzed simultaneously while fitting independent apparent dissociation constants (Figure 5B). Since the complex between a nine-residue CR2-derived E7 peptide and the pRB small pocket (nearly identical to the pRB_{his} domain described here) has a dissociation constant of 110 nM (*46*), it is reasonable to expect that the truncated proteins in this study have dissociation constants of 110 nM or lower. This assumption is further supported by the fact that a larger HPV16 E7/pRB60 complex has a dissociation constant in the low nanomolar range (*29*). On the basis of these data, it is reasonable to expect that very low to undetectable levels of $pRB_{his}/E7_{CR2-3}$ dissociation occurred during this experiment. Using this assumption, we fit a model containing three $E7_{CR2-3}/pRB_{his}$ complexes with 1:1, 2:2 and 4:4 molar stoichiometry. The apparent dissociation constants were 0.83 ± 0.52 μM for 1:1−2:2 molar equilibrium [$K_{d(1:1-2:2)}$] and 38 ± 25 μM for the 2:2−4:4 molar equilibrium [$K_{d(2:2-4:4)}$, Table 1]. This fit was significantly better than the fit for a model describing 1:1−2:2−3:3 oligomerization or fits with models describing 1:2 $E7_{CR2-3}/pRB_{his}$ molar ratios. However, models describing a molar ratio of 2:1 for the $E7_{CR2-3}/pRB_{his}$ complex fit only marginally worse than models describing 1:1 stoichiometry. Therefore, these experiments were unable to definitively establish the stoichiometry of the $E7_{CR2-3}/pRB_{his}$ complex. Nonetheless, both the $M_{w,app}$ and the multiple species models for this study demonstrate that the primary oligomerization state for the complex is greater than 1:1. In addition, the self-association models suggest that the predominant oligomerization state of the complex consists of two molecules of pRB_{his} and two or four molecules of $E7_{CR2-3}$.

Purification and Sedimentation Equilibrium Experiments of Recombinant $pRB_{his}/E1A_{CR1-3}$ Complex. The $E1A_{CR1-3}$ construct (Figure 1B), containing the minimal pRB-binding domain (CR2) and the second pRB-binding site (CR1), was coexpressed with pRB_{his} in bacteria as described (*69*). The complex was expressed at 15 °C (*69*). The proteins existed in the soluble fraction and were copurified through a combination of affinity chromatography (nickel agarose) and size-exclusion chromatography using a high load Superdex 200 prep-grade gel filtration column. The proteins coeluted from the gel filtration column at a molecular mass that is slightly larger than the 44 kDa protein standard and the individually purified pRB_{his} protein (Figure 6A). Since the expected molecular mass of a 1:1 molar $pRB_{his}/E1A_{CR1-3}$ complex is 67.1 kDa, the elution point of this complex is consistent with a complex of 1:1 stoichiometry (Figure 6A). This purification protocol was performed multiple times with highly reproducible results.

Two single speed sedimentation equilibrium experiments from two different protein preparations were performed with the $pRB_{his}/E1A_{CR1-3}$ complex at 18 500 and 18 700 rpm using interference optics. Three different starting concentrations were loaded for each experiment, providing six different samples for data analysis. After all of the protein samples reached equilibrium, the six data plots representing the protein concentration versus radius were fitted to a single species model to determine the overall $M_{w,app}$ of 80.2 kDa for the system (Table 1), suggesting that slight oligomer-

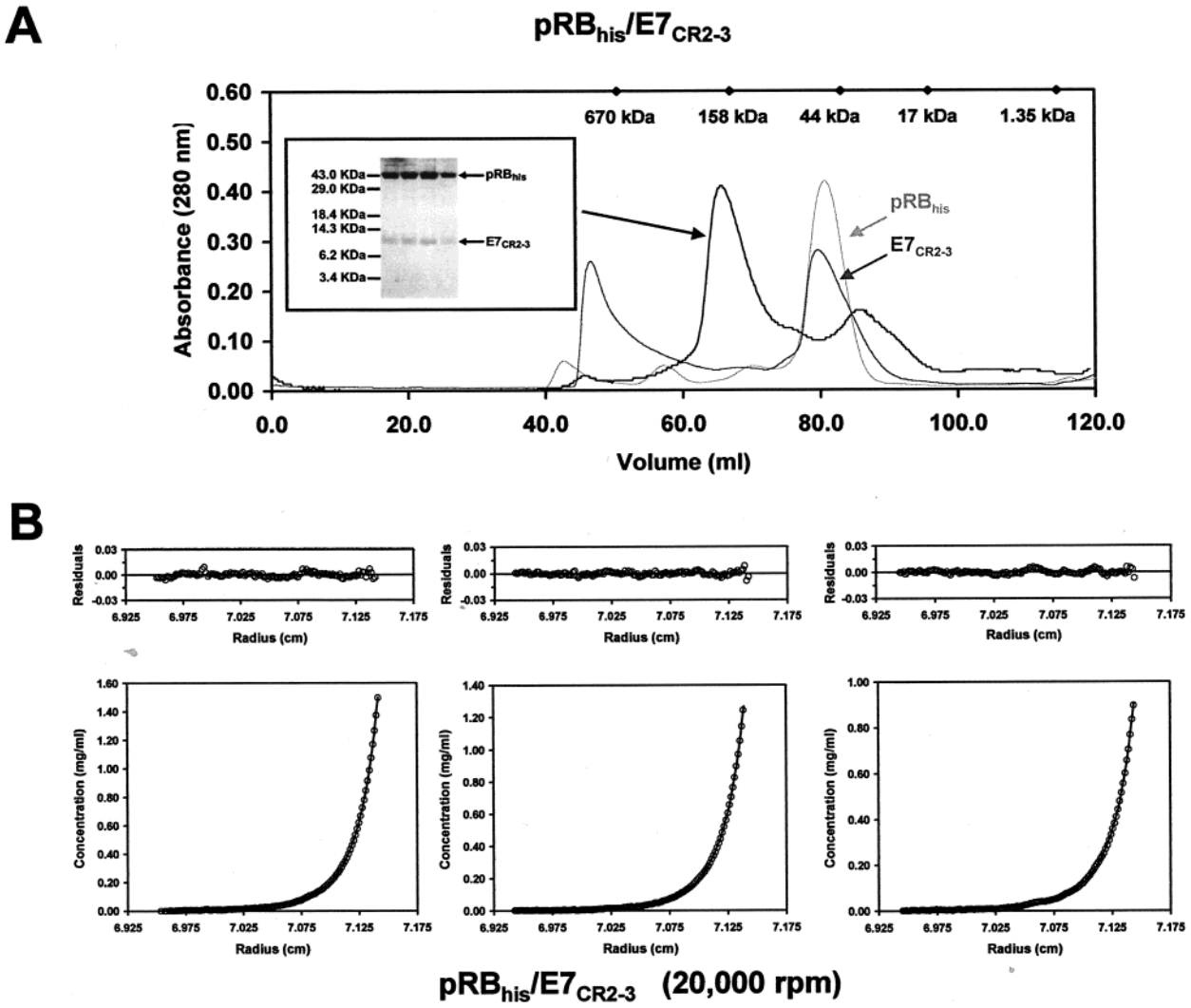

FIGURE 5: Predominant oligomeric state of the pRB$_{his}$/E7$_{CR2-3}$ complex has greater than 1:1 stoichiometry. (A) The final purification step of the recombinant pRB$_{his}$/E7$_{CR2-3}$ complex using size-exclusion chromatography. An 18% Coomassie-blue stained SDS−PAGE analysis of four peak fractions reveal that coexpressed recombinant pRB$_{his}$ and E7$_{CR2-3}$ coelute from a high load Superdex 200 prep-grade gel filtration column at approximately the elution point of the 158 kDa protein standard. A 1:1 stoichiometric complex consisting of pRB$_{his}$ and E7$_{CR2-3}$ has a calculated molecular mass of 59.3 kDa based on the protein sequences. The light gray peak represents the elution point of pRB$_{his}$ alone (the peak height is scaled down to facilitate peak elution point comparison). The dark gray peak represents the elution point of E7$_{CR2-3}$ alone (the peak height scaled down as well). (◆) The peak elution points of protein standards are represented. (B) Sedimentation equilibrium analysis of the purified pRB$_{his}$/E7$_{CR2-3}$ complex. Two separate 4 °C single speed sedimentation equilibrium experiments from separately purified complexes were performed at 18 000 and 20 000 rpm. Fringe displacement data from three different concentrations at both speeds were analyzed simultaneously with a model describing complexes of 1:1, 2:2 and 4:4 stoichiometry using NONLIN (*70*). The samples from the 20 000 rpm experiment are shown. This fit was significantly better than the fits for a model describing complexes of 1:1, 2:2, and 3:3 oligomerization and a model describing 2:1 pRB$_{his}$/E7$_{CR2-3}$ stoichiometry. However, the fit quality for pRB$_{his}$/E7$_{CR2-3}$ complexes of 1:2 stoichiometry was statistically equivalent to the fit shown. (○) Data points are represented. The top three panels represent the residuals for the calculated fits.

ization of a 1:1 pRB$_{his}$/E1A$_{CR1-3}$ complex was present. The six data plots were then fitted with models describing self-association using nonlinear regression (*70*). The six samples were analyzed simultaneously, while fitting individual apparent dissociation constants, to develop a model for reversible association (Figure 6B). For this model, it is assumed that pRB$_{his}$/E1A$_{CR1-3}$ dissociation is not present during the experiment because both previously defined pRB-binding sites are present within this E1A domain (*30*) and because the CR2 region has a significant degree of sequence homology with the E7 CR2-derived peptide mentioned previously. On the basis of the gel filtration elution profile of the complex, a 1:1 molar ratio of pRB$_{his}$/E1A$_{CR1-3}$ was assumed for first model and the apparent dissociation constant [$K_{d(1:1-2:2)}$] for the 1:1−2:2 equilibrium was 110 ± 56 μM (Table 1). In support of these results, this model of 1:1−2:2 oligomerization was significantly better than models describing either 2:1 or 1:2 molar ratios of pRB$_{his}$ to E1A$_{CR1-3}$. Unlike the larger pRB$_{his}$/E7$_{CR2-3}$ oligomerization state, the predominant oligomerization state in this system is one molecule of pRB$_{his}$ to one molecule of E1A$_{CR1-3}$.

DISCUSSION

We have used sedimentation equilibrium experiments to show that E1A$_{CR2-3}$ and E7$_{CR1-3}$ both participate in reversibly associating processes with significantly different dissociation constants (Table 1). At the concentrations tested, E7$_{CR1-3}$ exists as monomers, dimers, and tetramers while only reversible monomer−dimer association is detected for E1A$_{CR2-3}$. The apparent $K_{d(monomer-dimer)}$ of E1A$_{CR2-3}$ is 140

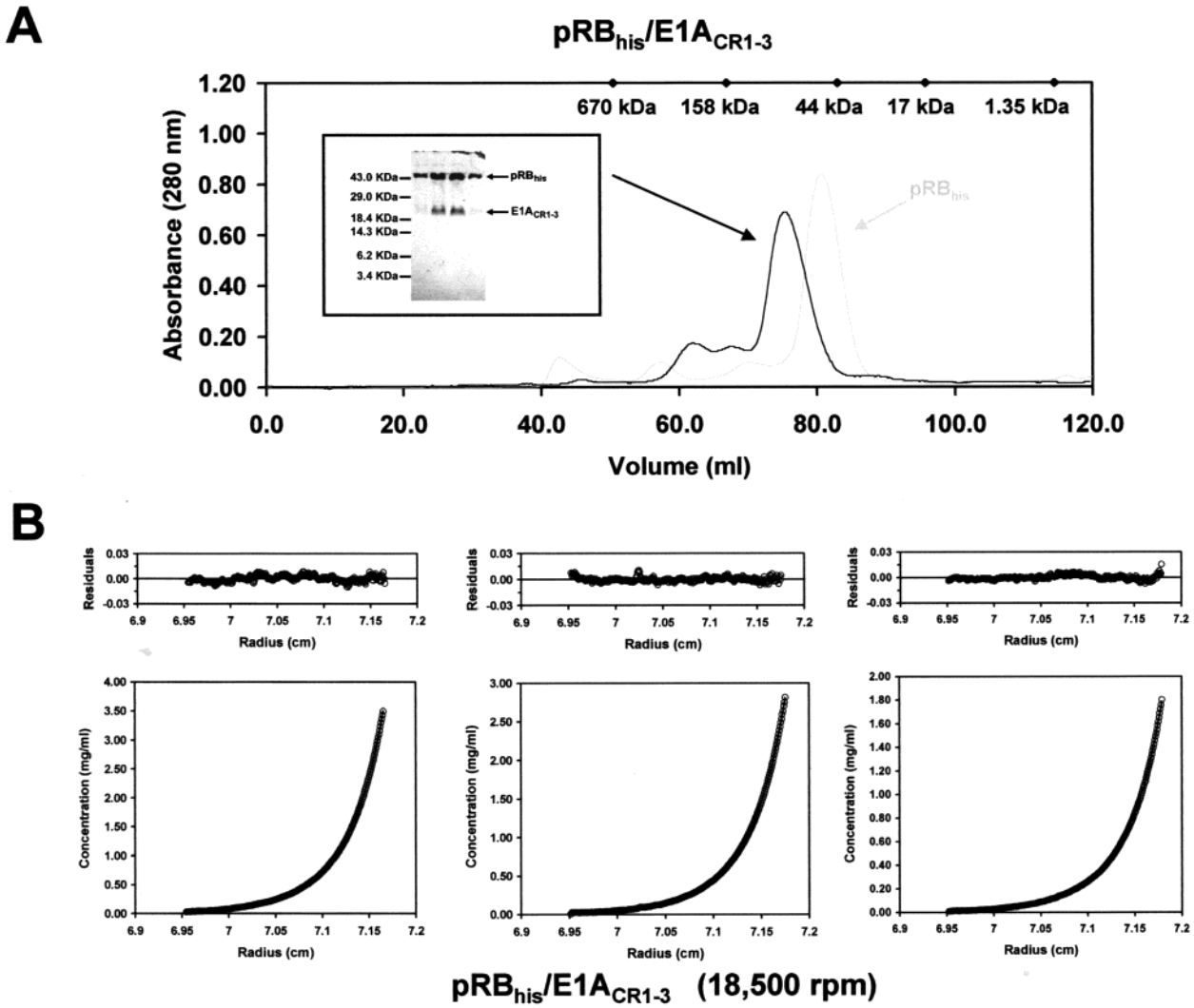

FIGURE 6: Purified recombinant pRB$_{his}$/E1A$_{CR1-3}$ complex exists predominantly with 1:1 stoichiometry. (A) The final purification step of the recombinant pRB$_{his}$/E1A$_{CR1-3}$ complex using size-exclusion chromatography. An 18% Coomassie-blue stained SDS−PAGE analysis of four peak fractions reveal that coexpressed recombinant pRB$_{his}$ and E1A$_{CR1-3}$ coelute from a high load Superdex 200 prep-grade size-exclusion column between elution points of protein standards with molecular masses of the 44 and 158 kDa. A 1:1 stoichiometric complex consisting of pRB$_{his}$ and E1A$_{CR1-3}$ has a calculated molecular mass of 67.1 kDa based on the protein sequences. The gray peak represents the elution point of pRB$_{his}$ alone (the peak height is scaled down to facilitate peak elution point comparison). (◆) The peak elution points of protein standards are represented. (B) Sedimentation equilibrium analysis of the pRB$_{his}$/E1A$_{CR1-3}$ complex from two speed and multiple protein concentrations. Two single speed sedimentation equilibrium experiments were performed at 18 500 and 18 700 rpm at 4 °C. Each experiment was performed with separately prepared complex. Fringe displacement data of six samples from different loading concentrations and/or speeds were analyzed simultaneously with a model describing complexes of 1:1 and 2:2 stoichiometry using NONLIN (*70*). Samples from the experiment at 18 500 rpm are shown. The bottom panel illustrates the calculated fits as continuous lines. (○) Data points for all scans are represented. The top three panels represent residuals for the calculated fits.

± 52 μM, which is approximately 100-fold higher than the apparent $K_{d(monomer-dimer)}$ of 1.1 μM for E7$_{CR1-3}$ (Table 1), demonstrating that at physiological protein concentrations, E1A$_{CR2-3}$ exists primarily as a monomer, while E7$_{CR1-3}$ exists primarily as a dimer. A comparison of the sedimentation equilibrium data with gel filtration elution profiles also suggests that the E7$_{CR1-3}$ dimer has an elongated shape because the E7$_{CR1-3}$ hydrodynamic radius is significantly larger than what is expected for a globular dimeric protein of a molecular mass of 22 kDa (Figure 2A). Since the E1A$_{CR2-3}$ monomer also elutes from gel filtration at a molecular mass significantly higher than its predicted monomeric molecular mass of 8.77 kDa (Figure 3A), it is likely that E1A$_{CR2-3}$ also adopts an elongated shape in solution.

The E7$_{CR2-3}$ gel filtration elution profile suggests that this domain has oligomerization properties and a shape similar to E7$_{CR1-3}$ (Figure 2A). This data supports the results of previous studies, which demonstrate that the oligomerization domain of HPV E7 is in the CR3 zinc-binding region (*27*, *51*, *68*). Despite the existence of similar zinc-binding motifs within the Ad E1A and HPV E7 CR3 regions, our studies with the E1A$_{CR2-3}$ protein show that the Ad E1A CR3 region is distinct from that of HPV E7 in that it does not mediate strong self-association. However, it is interesting to note that under the same buffer conditions, purified E1A$_{CR1-3}$ elutes from a gel filtration column as a series of aggregates (data not shown) while E1A$_{CR2-3}$ elutes in a single peak. This suggests that a domain between the beginning of CR1 and CR2 (amino acids 36−113) is responsible for E1A$_{CR1-3}$ aggregation, although the biological significance of this aggregation is unclear.

The gel filtration elution profile of the $pRB_{his}/E7_{CR2-3}$ complex suggests that the stoichiometry of binding is greater than 1:1 (Figure 5A) or that the complex adopts an elongated asymmetric shape in solution. Sedimentation equilibrium experiments with the $pRB_{his}/E7_{CR2-3}$ complex demonstrates that the molecular weight of the major species in solution is greater than that of a 1:1 stoichiometric complex. However, testing of 1:1 and of 1:2 $pRB_{his}/E7_{CR2-3}$ molar ratio models reveals no significant difference between the fit quality for the two possible $pRB_{his}/E7_{CR2-3}$ molar ratios. There are two main reasons for this. First, there is only a small difference between the molecular masss of the possible $pRB_{his}/E7_{CR2-3}$ molar ratios, with 1:1 and 1:2 estimated to be 58.6 and 67.4 kDa, respectively. Second, this complex appears to participate in a reversibly associating system with three different species detected for each model, resulting in a complicated system that can accommodate a variety of molar ratios. Therefore, we can only conclude from this experiment that the primary complex in the system contains two molecules of pRB_{his} and two or four molecules of $E7_{CR2-3}$. Since pRB_{his} alone is monomeric in solution, it appears that $E7_{CR2-3}$ is promoting the oligomerization of the $pRB_{his}/E7_{CR2-3}$ complex.

Unlike the $pRB_{his}/E7_{CR2-3}$ complex, the gel filtration elution profile of the $pRB_{his}/E1A_{CR1-3}$ complex demonstrates that this complex exists primarily with 1:1 stoichiometry (Figure 6A). Since the coexpressed $pRB_{his}/E1A_{CR1-3}$ complex elutes from the gel filtration column as a single peak (Figure 6A), it is probable that the presence of pRB_{his} is inhibiting the amino terminal-mediated $E1A_{CR1-3}$ aggregation observed when it is individually purified (data not shown). The sedimentation equilibrium experiment of this complex demonstrates that $pRB_{his}/E1A_{CR1-3}$ undergoes a weak reversible self-association between a 1:1 and 2:2 stoichiometric complex. The apparent dissociation constant for this oligomerization is similar to that of $E1A_{CR2-3}$ alone, raising the possibility that this relatively weak $pRB_{his}/E1A_{CR1-3}$ oligomerization is mediated through the CR2−CR3 region of Ad5 E1A (Table 1).

In summary, despite the overall functional similarities between the HPV16 E7 and Ad5 E1A proteins, we have elucidated distinct oligomerization properties of these DNA viral oncoproteins. We find that HPV16 $E7_{CR1-3}$ is predominantly dimeric at physiological concentrations while Ad5 $E1A_{CR2-3}$ is predominantly monomeric. Furthermore, the different CR3-mediated viral oncoprotein oligomerization states do not appear to be disrupted by pRB-binding. Therefore, differences between the oligomerization properties of Ad E1A and HPV E7 may be related to their distinct mechanisms of pRB-inactivation.

ACKNOWLEDGMENT

The authors wish to thanks David W. Speicher, Gillian E. Begg, Sandra L. Harper, and the National Analytical Ultracentrifugation Facility (Biotechnology Center, University of Connecticut) for technical advice, and to David W. Speicherfor critical reading of the manuscript.

REFERENCES

1. Chen, P., Riley, D. J., and Lee, W. (1995) *Crit. Rev. Eukaryotic Gene Expression 5*, 79−95.
2. Harbour JW, D. D. (2000) *Nat. Cell Biol. 2* E65-E67.
3. Helin, K., Lees, J. A., Vidal, M., Dyson, N., Harlow, E., and Fattaey, A. (1992) *Cell 70*, 337−350.
4. Helin, K., Harlow, E., and Fattaey, A. (1993) *Mol. Cell. Biol. 13*, 6501−6508.
5. Kaelin, W. G., Krek, W., Sellers, W. R., DeCaprio, J. A., Ajchenbaum, F., Fuchs, C. S., Chittenden, T., Li, Y., Farnham, P. J., Blanar, M. A., Livingston, D. M., and Flemington, E. K. (1992) *Cell 70*, 351−364.
6. Shan, B., Zhu, X., Chen, P.-L., Durfee, T., Yang, Y., Sharp, D., and Lee, W.-H. (1992) *Mol. Cell. Biol. 12*, 5620−5631.
7. Brehm, A. M. E., McCance, D. J., Reid, J. L., Bannister, A. J., and Kouzarides, T. (1998) *Nature 391*, 597−601.
8. Luo, R. X. P. A., and Dean, D. C. (1998) *Cell 92*, 601−605.
9. Magnaghi-Jaulin, L. G. R., Naguibneva, I., Robin, P., Lorain, S., Le Villain, J. P., Troalen, F., Trouche, D., and Harel-Bellan, A. (1998) *Nature 391*, 601−605.
10. Hensey, C. E., Hong, F., Durfee, T., Qian, Y. W., Lee, E. Y., and Lee, W. H. (1994) *J. Biol. Chem. 269*, 1380−1387.
11. Chow, K. N. B., and Dean, D. C. (1996) *Mol. Cell. Biol. 16*, 4862−4868.
12. Starostik, P., Chow, K. N. B., and Dean, D. C. (1996) *Mol. Cell. Biol. 16*, 3606−3614.
13. Hiebert, S. W. (1993) *Mol. Cell. Biol. 13*, 3384−3391.
14. Qian, Y., Luckey, C., Horton, L., Esser, M., and Templeton, D. J. (1992) *Mol. Cell. Biol. 12*, 5363−5372.
15. Qin, X.-Q., Chittenden, T., Livingston, D. M., and Kaelin, W. G. (1992) *Genes Dev. 6*, 953−964.
16. Wang, J. Y. J., Knudsen, E. S., and Welch, P. J. (1994) *Adv. Cancer Res. 64*, 25−85.
17. Hu, Q., Dyson, N., and Harlow, E. (1990) *EMBO J. 9*, 1147−1155.
18. Huang, S., Wang, N. P., Tseng, B. Y., Lee, W.-H., and Lee, E. Y.-H. P. (1990) *EMBO J. 9*, 1815−1822.
19. Dyson, N., Howley, P. M., Münger, K., and Harlow, E. (1989) *Science 243*, 934−937.
20. Dyson, N., Guida, P., Münger, K., and Harlow, E. (1992) *J. Virol. 66*, 3893−6902.
21. Chellapan, S., Kraus, V. B., Kroger, B., Münger, K., Howley, P. M., Phelps, W. C., and Nevins, H. R. (1992) *Proc. Natl. Acad. Sci. U.S.A. 89*, 4549−4553.
22. Huang, P. S., P. D., Edwards, G., Goodhart, P. J., Huber, H. E., Miles, L., Garsky, V. M., Oliff, A., and Heimbrook, D. C. (1990) *Mol. Cell Biol. 13*, 953−960.
23. Phelps, W. C., Yee, C. L., Munger, K., and Howley, P. M. (1988) *Cell 53*, 539−547.
24. Morozov, A., Shiyanov, P., Barr, E., Leiden, J. M., and Raychaudhuri, P. (1997) *J. Virol. 71*, 3451−3457.
25. Reusch, M. N., and Laimins, L. A. (1997) *J. Virol. 71*, 5570−5578.
26. Phelps, W. C., Münger, K., Yee, C. L., Barnes, J. A., and Howley, P. M. (1992) *J. Virol. 66*, 2418−2427.
27. Clemens, K. E., Brent, R., Gyuris, J., and Münger, K. (1995) *Virol. 241*, 289−293.
28. Jones, R. E., Wegrzyn, R. J., Patrick, D. R., Balishin, N. L., Vuicolo, G. A., Riemen, M. W., Defeo-Jones, D., Garsky, V. M., Heimbrook, D. C., and Oliff, A. (1990) *J. Biol. Chem. 265*, 12782−12785.
29. Jones, R. E., Heimbrook, D. C., Huber, H. E., Wegrzyn, R. J., Rotberg, N. S., Stauffer, K. J., Lumma, P. K., Garsky, V. M., and Oliff, A. (1992) *J. Biol. Chem. 267*, 908−912.
30. Dyson, N., Guida, P., McCall, C., and Harlow, E. (1992) *J. Virol. 66*, 4606−4611.
31. Egan, N., Jelsoma, T. N., Howe, J. A., Bayley, S. T., Ferguson, B., and Branton, P. E. (1988) *Mol. Cell. Biol. 8*, 3955−3959.
32. Whyte, P., Williamson, N. M., and Harlow, E. (1989) *Cell 56*, 67−75.
33. Seedorf, K., Oltersdorf, T., Krammer, G., and Rowekamp, W. (1987) *EMBO J. 6*, 139−144.
34. Von Knebel Doeberitz, M., Bauknecht, T., Bartsch, D., and Zur Hausen, H. (1991) *Proc. Natl. Acad. Sci. U.S.A. 88*, 1411−1415.
35. Heck, D. V., Yee, C. L., Howley, P. M., and Munger, K. (1992) *Proc. Natl. Acad. Sci. U.S.A. 89*, 4442−4446.

36. Sang, B.-C., and Barbosa, M. S. (1992) *Proc. Natl. Acad. Sci. U.S.A. 89*, 8063−8067.
37. Watanabe, S., Kanda, T., Sato, H., Furuno, A., and Yoshiike, K. (1990) *J. Virol. 64*, 207−214.
38. Munger, K., Yee, C. L., Phelps, W. C., Pietenpol, J. A., Moses, H. L., and Howley, P. M. (1991) *J. Virol. 65*, 3943−3948.
39. Edmonds, C., and Vousden, K. H. (1989) *J. Virol. 63*, 2650−2656.
40. Chesters, P. M., Vousden, K. H., Edmonds, C., and McCance, D. J. (1990) *J. Gen. Virol. 71*, 449−453.
41. Ressing, M. E., de Jong, J. H., Brandt, R. M. P., Drijfhout, J. W., Benckhuijsen, W. E., Schreuder, G. M. T., Offringa, R., Kast, W. M., and Melief, C. J. M. (1999) *Eur. J. Immunol. 29*, 1292−1303.
42. Greenstone, H. L., Nieland, J. D., de Visser, K. E., De Bruijn, M. L. H., Kirnbauer, R., Roden, R. B. S., Lowy, D. R., Kast, W. M., and Schiller, J. T. (1998) *Proc. Natl. Acad. Sci. U.S.A. 95*, 1800−1805.
43. Schafer, K., Muller, M., Faath, S., Henn, A., Osen, W., Zentrgaf, H., Benner, A., Gissmann, L., and Jochmus, I. (1999) *Int. J. Cancer 91*, 428−437.
44. Ressing, M. E., van Driel, W. J., Brandt, R. M. P., Kenter, G. G., de Jong, J. H., Bauknecht, T., Fleuren, G.-J., Hoogerhout, P., Offringa, R., Sette, A., Celis, e., Grey, H., Trimbos, B. J., Kast, M., and Melief, C. J. M. (2000) *J. Immunother. 23*, 255−266.
45. Liu, D.-W., Tsao, Y. P., Kung, J. T., Ding, Y.-A., Sytwu, H.-K., Xiao, X., and Chen, S.-L. (2000) *J. Virol. 74*, 2888−2894.
46. Lee, J.-O., Russo, A. A., and Pavletich, N. P. (1998) *Nature 391*, 859−865.
47. Ikeda, M.-A., and Nevins, J. (1993) *Mol. Cell. Biol. 13*, 7029−7035.
48. Webster, L. C., and Ricciardi, R. P. (1991) *Mol. Cell. Biol. 11*, 4287−4296.
49. Culp, J. S., Webster, L. C., Friedman, D. J., Smith, C. L., Huang, W.-J., Wu, F. Y.-H., Rosenberg, M., and Ricciardi, R. P. (1988) *Proc. Natl. Acad. Sci. U.S.A. 85*, 6450−6454.
50. Martin, K. J., Lillie, J. W., and Green, M. R. (1990) *Nature 346*, 147−152.
51. McIntyre, M. C., Frattini, M. G., Grossmon, S. T., and Laimons, L. A. (1993) *J. Virol. 67*, 3142−3150.
52. Pahel, G., Aulabaugh, A., Short, S. A., Barnes, J. A., Painter, G. R., Ray, P., and Phelps, W. C. (1993) *The J. Biol. Chem. 268*, 26018−26025.
53. Patrick, D. R., Zhang, K., Defeo-Jones, F., Vuocolo, G. R., Maigetter, R. Z., Sardana, M. K., Oliff, A., and Heimbrook, D. C. (1992) *The J. Biol. Chem. 267*, 6910−6915.
54. Massimi, P., Pim, D., Storey, A., and Banks, L. (1996) *Oncogene 12*, 2325−2330.
55. Phillips, A. C., and Vousden, K. H. (1997) *J. Gen. Biol. 78*, 905−909.
56. Horikoshi, N., Maguire, K. J., Kralli, A., Maldonado, E., Reinberg, D., and Weinmann, R. (1991) *Proc. Natl. Acad. Sci. U.S.A. 88*, 5124−5128.
57. Lee, W. S., Kao, C. C., Bryant, G. O., Liu, X., and Berk, A. J. (1991) *Cell 67*, 365−376.
58. Geisberg, J. V., L. W., Berk, A. J., and Ricciardi, R. P. (1994) *Proc. Natl. Acad. Sci. U.S.A. 91*, 2488−2492.
59. Boyer, T. G., M. M., Lees, E., Ricciardi, R. P., and Berk, A. J. (1999) *Nature 399*, 276−279.
60. Wang, H.-G. H., Rikitake, Y., Carter, M. C., Yaciuk, P., Abraham, S. E., Zerler, B., and Moran, E. (1993) *J. Virol. 67*, 476−488.
61. Stirdivant, S. M., Huber, H. E., Patrick, D. R., Defeo-Jones, D., McAvoy, E. M., Garsky, V. M., Oliff, A., and Heimbrook, D. C. (1992) *Mol. Cell. Biol. 12*, 1905−1914.
62. Huang, P. S., Patrick, D. R., Edwards, G., Goodhart, P. J., Huber, H. E., Miles, L., Garsky, V. M., Oliff, A., and Heimbrook, D. C. (1993) *Mol. Cell. Biol. 13*, 953−960.
63. Patrick, D. R., Oliff, A., and Heimbrook, D. C. (1994) *The J. Biol. Chem. 269*, 6842−6850.
64. Boyer, S. N., Wazer, D. E., and Band, V. (1996) *Cancer Res. 56*, 4620−4624.
65. Berezutskaya, E., Yu, B., Morozov, A., Raychaudhuri, P., and Bagchi, S. (1997) *Cell Growth Differ.* 1277−1286.
66. Jones, D. L., and Münger, K. (1997) *J. Virol. 71*, 2905−2912.
67. Chinami, M., Sasaki, S., Hachiya, N., Yuge, K., Ohsugi, T., Maeda, H., and Shingu, M. (1994) *J. Gen. Virol. 75*, 277−281.
68. Zwerschke, W., Joswig, S., and Jansen-Durr, P. (1996) *Oncogene 12*, 213−220.
69. Johnston, K., Clements, A., Venkataramani, R. N., Trievel, R. C., and Marmorstein, R. *Protein Expression Purif.* (in press).
70. Johnson, M. L., Correia, J. J., Yphantis, D. A., and Halvorson, H. R. (1981) *Biophys. J. 36*, 575−588.
71. Laue, T. M., Shah, B., Ridgeway, T. M., and Pelletier, S. L. (1992) Computer-aided interpretation of analytical sedimentation data for proteins. *Analytical Ultracentrifugation in Biochemistry and Polymer Science*, Royal Society of Chemistry, Cambridge.
72. Yphantis, D. A. (1964) *Biochemistry 3*, 297−317.

BI002111G